Materials Science in Semiconductor Processing 153 (2023) 107133

Contents lists available at ScienceDirect

Materials Science in Semiconductor Processing

journal homepage: www.elsevier.com/locate/mssp

Improved electrical properties of encapsulated $MoTe_2$ with 1T′ edge contacts via laser irradiation

Yewon Kim [a], A. Venkatesan [a], Jihoon Kim [a], Hanul Kim [b], Kenji Watanabe [c], Takashi Taniguchi [d], Dongmok Whang [b,e], Gil-Ho Kim [a,b,*]

[a] Department of Electrical and Computer Engineering, Sungkyunkwan University (SKKU), Suwon, 16419, Republic of Korea
[b] Samsung-SKKU Graphene Centre, Sungkyunkwan Advanced Institute of Nanotechnology (SAINT), Sungkyunkwan University (SKKU), Suwon, 16419, Republic of Korea
[c] Research Center for Functional Materials, National Institute for Materials Science, 1-1 Namiki, Tsukuba, 305-0044, Japan
[d] International Center for Materials Nano-Architectonics, National Institute for Materials Science, 1-1 Namiki, Tsukuba, 305-0044, Japan
[e] Department of Advanced Materials and Engineering, Sungkyunkwan University (SKKU), Suwon, 16419, Republic of Korea

A B S T R A C T

Transition metal dichalcogenides (TMDCs) encapsulation is an essential technology for improving electron transport and preventing external contamination in practical applications. Nevertheless, Ohmic contacts in TMDCs continue to pose many problems. A laser was irradiated along with $MoTe_2$ encapsulated in h-BN and edge contact electrodes. We studied the properties of the edge contact resistance, in which the crystal structure of $MoTe_2$ changes from a semiconductor hexagonal phase (2H) to a metallic monoclinic phase (1T′). The contact between TMDCs and the metal electrode, Fermi-level pinning, contact resistance, and Schottky barrier height (SBH) can be calculated. Laser irradiation of the edge contact confirmed that, due to the change in the crystal structure of $MoTe_2$, a reduction in contact resistance by over a factor of three resulted in the development of the electrical properties of the device. Field-effect transistors (FETs) with indium (In) edge contact exhibit high performance, with the highest electron mobility reaching 7.9 $cm^2V^{-1}s^{-1}$ at 300 K. Furthermore, the barrier heights for In with a $MoTe_2$ junction were 10.3 meV after laser irradiation, which is more than ten times the low SBH. This study confirms the improved electrical properties of the two-dimensional material and metal were confirmed using a laser.

1. Introduction

The flexibility to engineer band gap in transition metal dichalcogenide (TMDC) along with its thickness-dependent electrical [1–3], thermal [4], mechanical [5], and optical properties [6–8] makes it one of the most interesting material systems till date. Additionally, TMDC shows polymorphism with diverse structural and electronic phases with metallic, semi metallic, and semiconducting characteristics. In particular, molybdenum ditelluride ($MoTe_2$) exists in all four electronic phases with hexagonal (2H), octahedral (1T), monoclinic (1T′), and orthorhombic (T_d) [9–14]. The 2H and 1T structures are predominantly semiconductors, whereas 1T' and T_d structures are semimetals.

Achieving Ohmic electrical contact with TMDCs is highly challenging. Contact problems have been highlighted as a central challenge in applications and basic studies. For instance, to reduce the Schottky barrier height (SBH) [15–18], studies conducted to identify metals with appropriate work functions based on the electron affinity of $MoTe_2$ have not been effective because of the strong Fermi-level pinning effect [19,20]. The presence of an abundant metal electrode near the conduction band has been shown to improve device performance due to effective carrier injection, thereby reducing contact resistance [21]. Various approaches have been explored to overcome this problem, including molecular doping, tunnel-barrier insertion, fabrication of graphene contacts, crystal damage, thermal annealing, and phase changes [22–25].

The contact resistance of $MoTe_2$ field-effect transistors (FETs) can be reduced by converting the $MoTe_2$ crystalline phase locally (source and drain) from 2H into 1T′ through laser irradiation [26–28]. Laser irradiation causes Te vacancies to produce unidirectional phases from 2H to 1T′, and a junction structure free of oxides or other elements [25]. This phase change reduces the SBH between $MoTe_2$ (laser irradiated source and drain) and the metal electrode, thereby solving the Schottky contact problem and improving device performance [29,30]. The low contact resistance of $MoTe_2$ through phase tuning by laser irradiation has been recently reported [31]. The ultra-thin semiconductor $MoTe_2$ nanosheet synthesized through chemical vapor deposition was locally irradiated with a laser to show improved electrical performance due to charge injection and demonstrated lower contact resistance, demonstrating the

* Corresponding author. Department of Electrical and Computer Engineering, Sungkyunkwan University (SKKU), Suwon 16419, Republic of Korea
E-mail address: ghkim@skku.edu (G.-H. Kim).

https://doi.org/10.1016/j.mssp.2022.107133
Received 30 December 2021; Received in revised form 4 August 2022; Accepted 25 September 2022
Available online 7 October 2022

superior performance of the 1T' $MoTe_2$ device compared to 2H $MoTe_2$. In addition to laser irradiation, we have demonstrated that indium could be an excellent metal option (similar to the work function of $MoTe_2$) for making low Schottky barrier height electrical contact on irradiated $MoTe_2$ [32]. And one-dimensional (1D) contact, one of the methods to obtain low contact resistance, is used. The laser is irradiated locally only to the electrode in contact with the material so that 2H and 1T′ phases can coexist in the $MoTe_2$ FET.

Recently, 1D contact with graphene and other TMDCs was demonstrated by evaporating a metal contact to an exposed edge of the channel material encapsulated between hexagonal boron nitride flakes [33–35]. This innovative approach achieves a low contact resistance in an architecture that minimizes extrinsic scattering in the channel. However, this architecture is not well studied and has not been tested or proven effective for $MoTe_2$.

In this study, we prepared 1D edge contacts between indium (In) and hexagonal boron nitride (h-BN) encapsulated $MoTe_2$. To understand the properties of 1D In junctions in $MoTe_2$, we performed temperature-dependent transfer measurements between 77 and 420 K. We found that 1D In contacts can effectively fabricate suitable Ohmic contacts with low contact resistance in $MoTe_2$ [36,37]. The contact resistance of the laser-irradiated device was 0.7 kΩ μm and decreased by a factor of approximately three from 2.2 kΩ μm before laser irradiation. This indicates that this technique is suitable for producing appropriate electrical contacts in $MoTe_2$.

2. Experimental section

Using an adhesive tape method, a ulk n-type $MoTe_2$ crystal (HQ graphene Inc.) was used for exfoliation on highly doped p-type Si with a 285 nm-thick SiO_2 layer. The suitable few-layer flakes were identified via optical microscopy. A suitable h-BN and few-layer $MoTe_2$ was constructed through the dry transfer technique using a polycarbonate (PC) film with PDMS. Then etched with CF_4/O_2 (1/10 sccm) gas using reactive ion etching plasma equipment after the electrode pattern for edge contact was fabricated using electron-beam lithography. The edge contact electrodes were deposited with In (20 nm)/Au (30 nm) deposition for In contact. Then, using Raman spectroscopy irradiated laser at the edge where $MoTe_2$ and electrode contact at 2.4 mW, with a wavelength of 532 nm, for 20 s.

3. Results and discussion

We exfoliated a few-layer $MoTe_2$ on a heavily doped p-type silicon wafer with a 285 nm thick SiO_2 using adhesive tape. Then, a suitable flake was identified via optical microscopy image. To encapsulate $MoTe_2$, suitable top and bottom h-BN flakes were exfoliated and identified. The h-BN/$MoTe_2$/h-BN heterostructure was constructed through the dry transfer technique using polydimethylsiloxane with a thin film of polycarbonate stamp [34]. The encapsulated five-layer $MoTe_2$ was annealed in a 10^{-6} Torr for 3 h at 200 °C to reduce the organic residues, impurities and remove the air bubbles formed at the interface of the h-BN/$MoTe_2$/h-BN heterostructure during dry transfer [36]. The electrode pattern for edge contact was fabricated using electron-beam lithography. The edge electrode part was subsequently etched with CF_4/O_2 (1/10 sccm) gas using reactive ion etching plasma equipment. The electrodes were deposited in an electron-beam evaporator at 1–2 Å/s, with a deposition pressure of 2×10^{-7} Torr. To understand the effect of laser irradiation, we exposed the 2H $MoTe_2$ to a laser at 2.4 mW, with a wavelength of 532 nm, for 20 s with a spatial of less than 1 μm. The laser was intensively irradiated to the electrode part in contact with $MoTe_2$ by edge contact. In this process, Te vacancies in $MoTe_2$ were formed, which led to a phase transition to the 1T′ phase. The reason for not irradiating directly on $MoTe_2$ was to check the effect of laser irradiation between the semiconductor material and the electrode by uniformly affecting only the element in direct contact with the electrode.

Fig. 1(a) shows a schematic diagram of the encapsulated $MoTe_2$ with 1D contact In/Au (20/30 nm) deposited by the electron-beam evaporator technique. After deposition, the sample was annealed with 1000 sccm argon gas at 150 °C for 2 h to ensure adequate adhesion of the electrodes. Laser irradiation of the contact region of the electrode with $MoTe_2$ induced the phase change from 2H to 1T′ in $MoTe_2$. Fig. 1(b)–(d) present the optical microscopy image of the h-BN encapsulated $MoTe_2$ device, atomic force microscopy (AFM) image of a five-layer $MoTe_2$ flake (thickness of 4.46 nm) [38], and Raman spectra of five-layer $MoTe_2$ obtained using a 532 nm laser at room temperature. In the 2H $MoTe_2$ Raman spectrum, the presence of the signature peaks of the out-of-plane mode A_g (~174 cm^{-1}), in-plane mode E^1_{2g} (~235 cm^{-1}), and bulk-inactive mode B_{2g} (~290 cm^{-1}) confirms that the flake used in this experiment is $MoTe_2$ [36,37]. The after laser-irradiated showed new peaks near 124 and 138 cm^{-1}, corresponding to the A_g mode on the 1T' phase as shown in Fig. 1(d) [3,25].

Fig. 2(a) shows the room temperature output characteristics of $MoTe_2$ FETs before laser irradiation, measured at different back-gate voltages from −40 to +40 V. During the transport measurements, the sample was kept under vacuum (20 mTorr). The output characteristic graphs are shown in Fig. 2(a) indicating the formation of Ohmic-like contacts. Fig. 2(b) shows the transfer characteristics of h-BN encapsulated $MoTe_2$ on both linear and logarithmic scales at a fixed drain voltage (V_D) of 1 V and a back-gate voltage (V_G) from −40 to +40 V. The transfer characteristics indicate that the h-BN encapsulated $MoTe_2$ exhibited ambipolar characteristics with the dominant n-type region. The on/off ratios of the n-type and hole regions were 10^5 and 10^4, respectively. Fig. S1 presents the properties of the $MoTe_2$ edge contact device not encapsulated with h-BN. Unprotected devices have shorter operating times and are more susceptible to contamination than protected devices. To understand the impact of laser irradiation, h-BN encapsulated $MoTe_2$ was irradiated with a laser. Laser irradiation was conducted at the edges of the contact electrodes, as shown in Fig. 1(a). For laser irradiation, the same laser parameters were followed as used for Raman spectra characterization. Fig. 2(c) and (d) show the laser-irradiated h-BN encapsulated $MoTe_2$ transistor properties. Fig. 2(c) shows the output characteristics of different values of V_G ranging from −60 to +60 V. After irradiation, the current improved significantly at a given drain voltage. Fig. 2(d) shows the transfer characteristics of h-BN encapsulated $MoTe_2$ in linear and logarithmic scales, with back gate V_G from −60 to +60 V, at a fixed V_D of 1 V. After laser irradiation, the hole region of the sample disappeared and became completely n-type. Moreover, a dramatic change in the on/off ratio was observed; the on/off ratio of the laser-irradiated (n-type region) device changed from 10^5 to 10^1. The decrease in the on/off ratio could be attributed to the phase transition of $MoTe_2$ in the active channel of the device (along with the phase transition at the edge contacts) due to the unintentional irradiation of the laser. Previous studies on laser-induced phase transition in $MoTe_2$ flakes have clearly explained how laser irradiation on the channel could dramatically change the on/off ratio in $MoTe_2$ [1]. It is suggested that the laser irradiation creates Te vacancy in $MoTe_2$ flakes in large numbers resulting in the alteration in the stoichiometry of the Mo atoms [38–40]. This leads to a reconstruction of its atomic structure and the phase transition of the 2H phase to the 1T′ phase (the appearance of A_g modes in Raman spectra (Fig. 1(c)) at ~127 and ~141 cm^{-1} are the direct evidence for 2H to 1T′ phase formation in $MoTe_2$). It is to be pointed out that during the laser irradiation at the metal contacts, it was difficult to control the position of the laser spot only at contact. We believe that it could have unintentionally affected the part of the channel, resulting in the low on/off ratio. However, we have observed more improved contact resistance in the laser irradiated device which is discussed with the temperature-dependent transport measurements in the later part of the manuscript (Fig. 4(b)). Currently, we are working on the various parameters in understanding the laser irradiation (laser power and position of the laser spot) of encapsulated $MoTe_2$ devices to

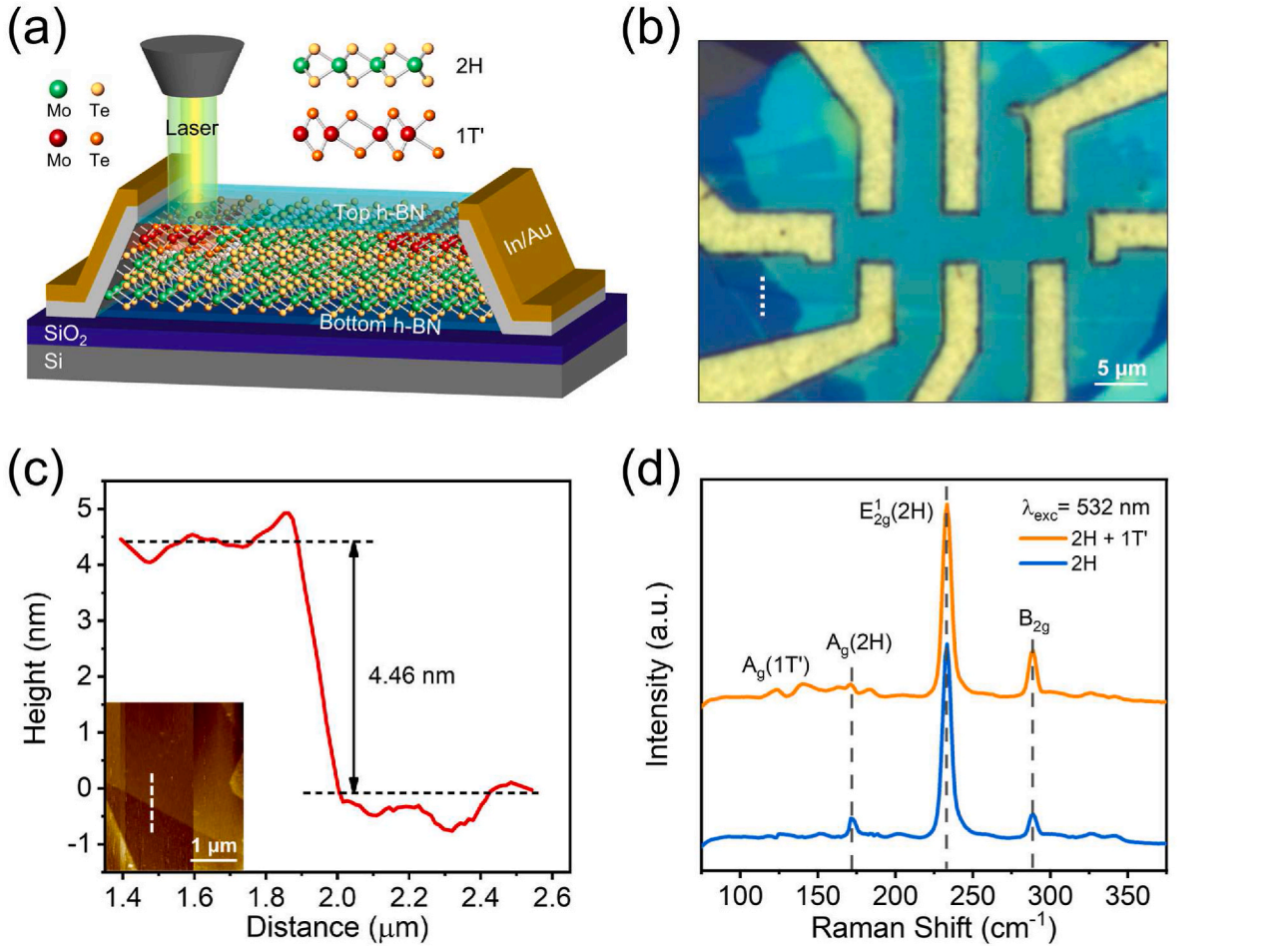

Fig. 1. (a) Schematic diagram of the laser irradiation process on the electrode edge of a $MoTe_2$ In/Au edge contact device encapsulated with h-BN. (b) Optical image of the device with In/Au contacts patterned by electron-beam lithography. (c) The height profile of the five-layer $MoTe_2$ flake is shown in (b). Inset shows the AFM image and line scan (dashed white line) of the $MoTe_2$ in the unencapsulated part. (d) Raman spectrum of five-layer 2H $MoTe_2$ before laser irradiation.

improve further both on/off ratio and contact resistances. Our initial results are promising and believe it can create new opportunities in this direction to further understand the effect of laser irradiation and the resulting electrical characteristics.

The temperature-dependent transport characteristics of h-BN encapsulated $MoTe_2$ were investigated at different temperatures in the range of 77–420 K. First, the sample was cooled to 77 K using liquid nitrogen. Then, all measurements were conducted by increasing the temperature at various intervals. The aforementioned procedure was performed both before and after laser irradiation to understand the modulation of contact resistances before and after laser irradiation for gate voltages from −9 to 0 V. Fig. 3(a) shows the temperature-dependent (77–420 K) transport characteristics of h-BN encapsulated $MoTe_2$ before laser irradiation. As the temperature increased from 77 to 420 K, the hole current also increased. Fig. 3(b) shows the transfer characteristics of the laser-irradiated device in the same temperature range. To calculate the SBH at the $MoTe_2$-metal interface, Arrhenius plots were plotted before and after laser irradiation. Fig. 3(c) and (d) show the Arrhenius plot of the h-BN encapsulated $MoTe_2$ device before and after laser irradiation [41,42]. Before irradiation, the graphs were plotted for a temperature range of 77–420 K for gate voltages from −9 to 0 V; the voltage range used after irradiation was −30 to −10 V. The change in slope can be observed by the Arrhenius plot of the irradiated laser device for an applied gate voltage V_G of −30 to −10 V (Fig. 3(d)). The transfer curve was used to plot $\ln(I_D/T^{3/2})$ as a function of $1000/T$. The slope of the linear fit yielded the SBH for a specific V_G, as shown in Fig. 3(e) and (f). The SBH for the electron transport is 175 meV at flat-band voltage $V_{FB} = -8.8$ V, as depicted in Fig. 3(e). The blue line indicates that the SBH for the hole transport at $V_{FB} = -10.4$ V is 311 meV. Fig. 3(f) shows that the SBH of the irradiated laser device for the electron transport is 10.3 meV at flat-band voltage $V_{FB} = -29$ V. The temperature ranges from 300 to 420 K, and carrier transfer curves were used to extract the SBH, which can be described via the thermionic emission equations in Schottky contact devices [45–47]. In these equations, $W$is the channel width, A^*_{2D} is the modified Richardson constant, q is the electron charge, $\varnothing_B$ is the SBH, k is the Boltzmann constant, V_D is the drain voltage, and m^* is the effective mass. We applied $V_D = 1$ V to $MoTe_2$ with an In 1D contact device. The $MoTe_2$ device showed ambipolar behavior in a strong n-branch with a small bandgap.

The contact resistance of the edge-contacted $MoTe_2$ before and after laser irradiation was calculated by conducting a four-terminal measurement. Fig. 4 shows the contact resistance ($R_{contact}$) and channel resistance ($R_{channel}$) of the edge contacted $MoTe_2$, measured at room temperature. The channel resistance was measured using four-point probe techniques, and the total resistance (R_{total}) was measured from the transfer characteristics between the same contacts. The contact resistance is extracted from the relation $R_{total} = 2R_{contact} + R_{channel}$. Fig. 4(a) and (b) show the channel, contact, and total resistances before and after laser irradiation, respectively. When the gate voltage V_G increased positively, the contact resistance decreased significantly in the before laser-irradiated sample. Generally, the contact resistance reduces by increasing the applied voltage; particularly, it decreases from 30.5 to 2.2 kΩ μm by increasing the gate voltage from 0 to 30 V. Accordingly, we observed the contact resistance of the laser-irradiated sample to

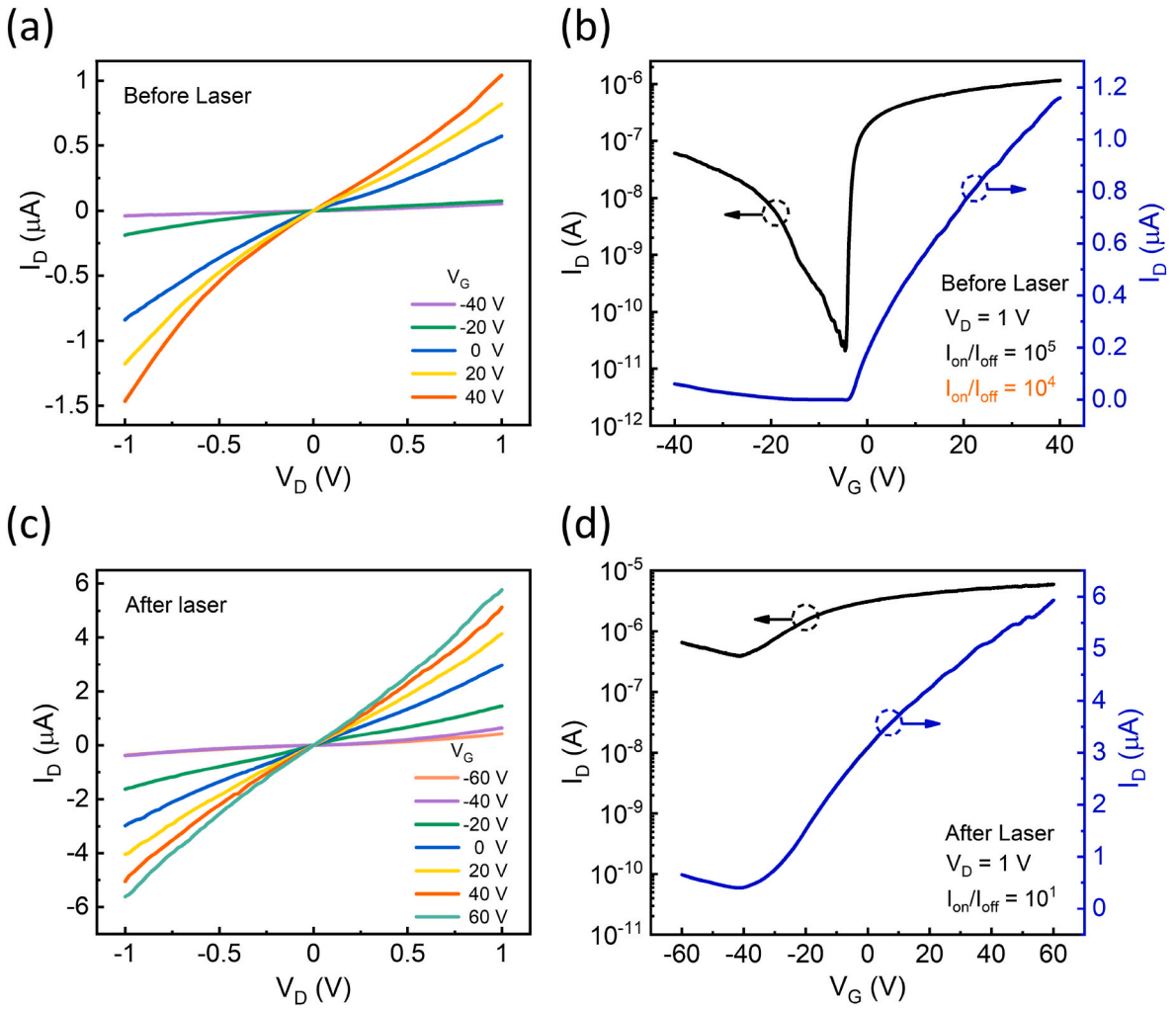

Fig. 2. Encapsulated $MoTe_2$ transistor properties at room temperature under vacuum. (a) Output characteristics of a before irradiated laser device at different gate voltages ranging from −40 to +40 V. (b) Transfer characteristics of pristine $MoTe_2$ with In contact a drain voltage of 1 V device. (c) Output characteristics of an after irradiated laser device for gate voltage ranging from −60 to +60 V. (d) Transfer characteristics of irradiated laser $MoTe_2$ at a drain voltage of 1 V.

decrease to 0.7 kΩ μm at V_G = 30 V, indicating the tendency of the contact resistance to further decrease due to laser irradiation.

The field-effect mobility (μ) can be calculated by $\mu = [L / (W \bullet C_i)] \times (dI_D / dV_G) \times (1 / V_D)$, where a fixed V_D = 1 V slope (dI_D / dV_G) is determined by the linear slope extracted from the experimental data [47–50]. $L = 15 \times 10^{-4}$ cm and $W = 3 \times 10^{-4}$ cm represents the length and width of the channel, respectively. C_i represents the capacitance, which is 1.21×10^{-8} F/cm^2. As shown in Fig. 5(a), the initial values (before laser irradiation) of electron mobility increased from 1.4 to 8.4 cm^{2}V^{-1}s^{-1} as the temperature increased from 77 to 380 K. Therefore, the method of process the device for the method of irradiating the laser only to the electrode so as not to affect the channel is shown in Fig. S3. The electrical characteristics and mobility after irradiating the laser only on the electrode were shown in Fig. S4. In addition, the threshold voltages are plotted in Fig. 3(a) and (b). As the temperature increased from 77 to 420 K, the devices exhibited a similar temperature dependence before and after laser irradiation, and we observed a negative shift in threshold voltages, as shown in Fig. 5(b). We also analysed our transport measurements using direct tunnelling (DT) and Fowler–Nordheim tunnelling (FNT). Tunnelling behavior can be classified as DT or FNT, according to the characteristics of the interfacial barrier; DT occurs when the barrier is trapezoidal, and FNT occurs when the barrier is triangular. DT and FNT can be expressed by the equations, $I_{DT} \propto V \exp(-4\pi d\sqrt{2m^*\varnothing_B}/h)$ and $I_{FNT} \propto V^2 \exp(-8\pi d\sqrt{2m^*\varnothing_B^3}/3ehV)$, respectively [43,44]. Here, d is tunnelling barrier thickness, m^* is carrier effective mass, $\varnothing_B$ is barrier height, and h is the Planck's constant. Fig. 5 (c) and (d) present a plot of $\ln(I_D/V_D^2)$ versus $1/V_D$ at a temperature ranging from 100 to 300 K and at zero gate voltage. FNT can be observed when the interfacial barrier is triangular, as mentioned earlier, and biased with a high drain voltage. This increases the probability that the carrier will pass through due to tunnelling [51–53]. Fig. 5(c) demonstrates the change in the transport mechanism from DT at low drain bias to FNT at high drain bias at the interface of the In edge contact $MoTe_2$ device. FNT can be observed at relatively low temperatures because of its mechanism of operation, which does not require thermal energy. DT was observed at a relatively lower electric field than the FNT. As shown in Fig. 5(d), DT was the dominant mechanism at various temperatures in the laser-irradiated device. After laser irradiation, no FNT was observed at the applied bias owing to a decrease in the SBH.

4. Conclusions

In conclusion, we demonstrated the use of In as a metal electrode for $MoTe_2$ 1D edge-contact devices encapsulated in h-BN. The van der Waals heterostructure using a high-vacuum thermal annealing process reduces interfacial impurities and improves contact with the electrode. Various temperature-dependent electrical transport measurements facilitate the implementation of highly mobile two-dimensional devices.

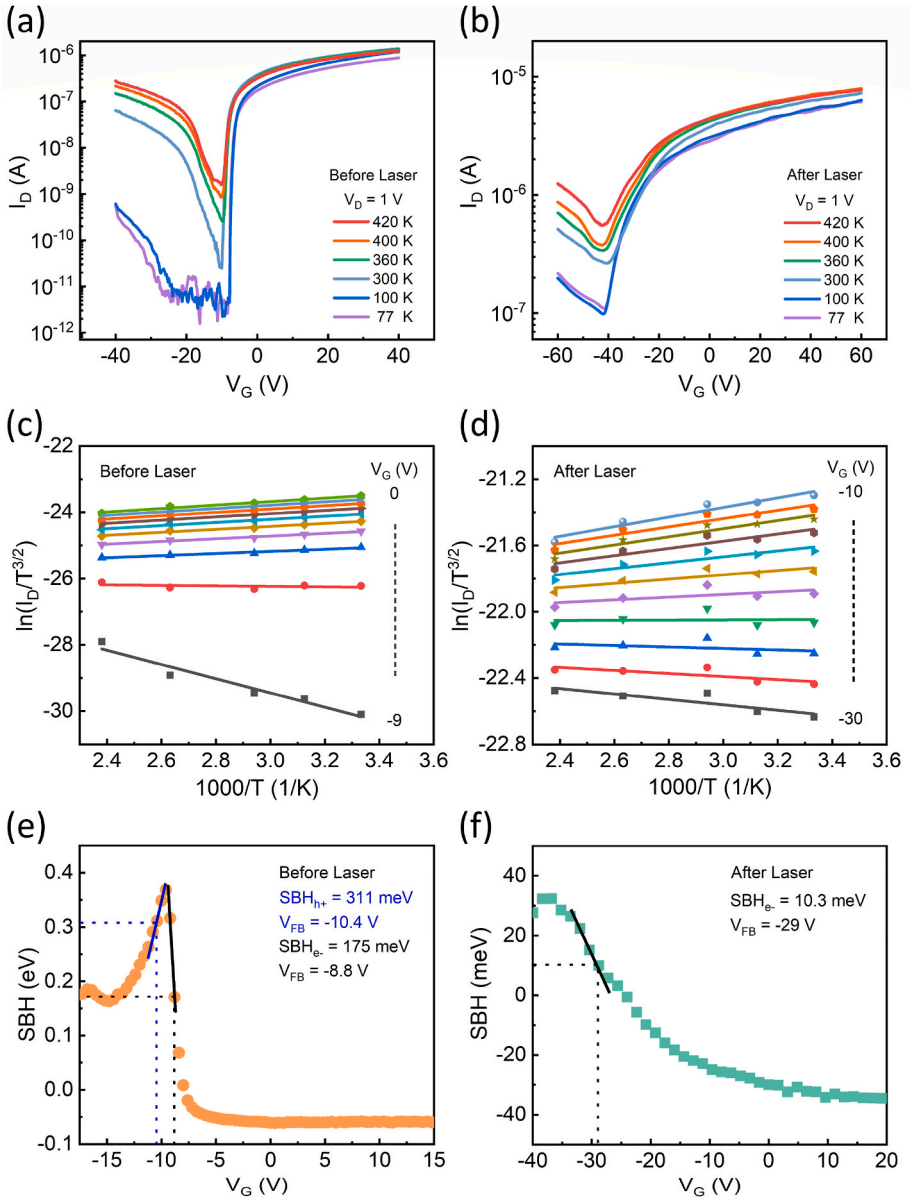

Fig. 3. (a) Temperature-dependent (77–420 K) transfer characteristics when the drain voltage is 1 V. (b) Temperature-dependent (77–420 K) transfer characteristics after laser irradiation. (c) Arrhenius plot, $\ln(I_D/T^{3/2})$, as a function of temperature based on the gate voltage from −8 to 0 V. (d) Arrhenius plot of irradiated laser device from −30 to −10 V. (e) SBH of 1D edge contact FET device plotted as a function of gate voltage. (f) SBH was obtained from a laser-irradiated device.

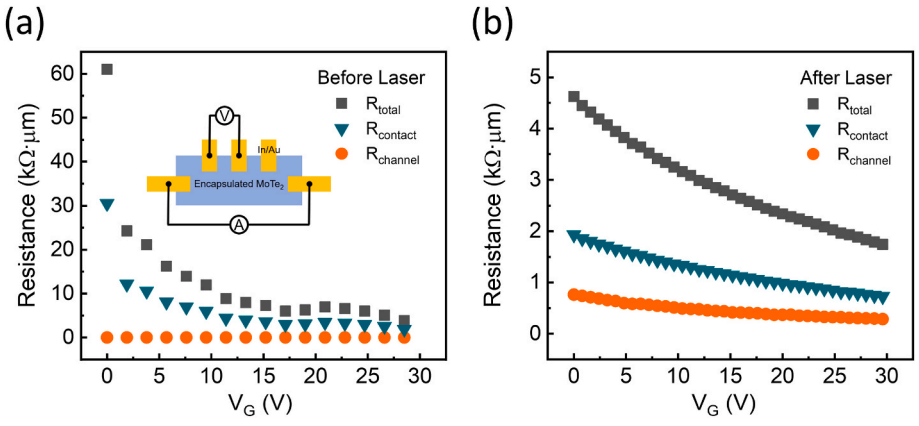

Fig. 4. Contact resistance at room temperature. (a) Total, channel, and contact resistances of h-BN encapsulated $MoTe_2$ device as a function of gate voltage V_G. Inset: The sketch of the measurement set-up used in the four-terminal measurement. (b) The contact resistance of the device after laser-irradiated device using the same electrode as that used in the device before laser irradiation. Variation in total, channel, and contact resistances of the laser-irradiated h-BN encapsulated $MoTe_2$ device as a function of gate voltage.

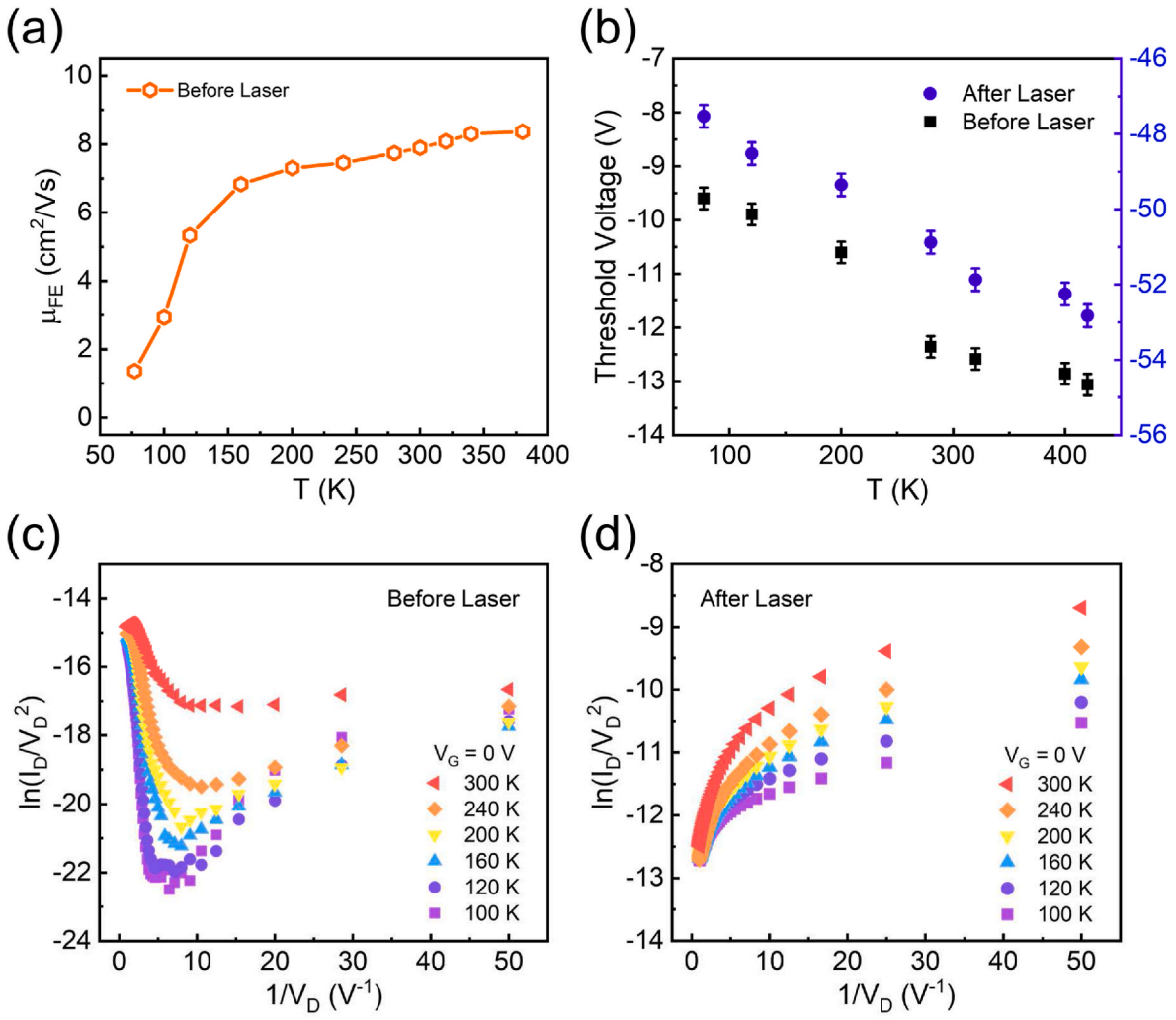

Fig. 5. (a) Variation in the mobility of h-BN encapsulated $MoTe_2$ device at temperatures ranging from 77 to 380 K. (b) Variation of the threshold voltage of h-BN encapsulated $MoTe_2$ device before and after laser irradiation at the same temperature range as in (a). (c) $\ln(I_D/V_D^2)$ as a function of $1/V_D$ at zero gate voltage at temperatures ranging from 100 to 300 K for the h-BN encapsulated $MoTe_2$ device. (d) $\ln(I_D/V_D^2)$ as a function of $1/V_D$ at zero gate voltage for the same temperature range as in (c) for a laser-irradiated h-BN encapsulated $MoTe_2$ device.

The SBH of the irradiated laser device for the electron transport is 10.3 meV at flat-band voltage $V_{FB} = -29$ V. The contact resistance of the laser-irradiated sample to decrease to 0.7 kΩ μm at $V_G = 30$ V, indicating the tendency of the contact resistance to further decrease due to laser irradiation. The laser-irradiated edge contact of the encapsulated material simultaneously solves the problem of contamination and improves contact resistance. The laser-irradiated $MoTe_2$ 1D edge contact exhibited better contact resistance compared to that without laser irradiation. Furthermore, similar to the work function of $MoTe_2$, In can also provide a low SBH. In this study, we presented a method for designing contacts to enhance charge transport performance and expand the applications of 2D materials and TMDCs in future devices.

CRediT authorship contribution statement

Yewon Kim: Writing – original draft, Visualization, Formal analysis, Data curation. **A. Venkatesan:** Writing – review & editing, Validation, Formal analysis. **Jihoon Kim:** Writing – review & editing, Formal analysis, Conceptualization. **Hanul Kim:** Methodology, Investigation, Conceptualization. **Kenji Watanabe:** Validation, Resources. **Takashi Taniguchi:** Validation, Resources. **Dongmok Whang:** Validation. **Gil-Ho Kim:** Writing – review & editing, Validation, Resources.

Declaration of competing interest

The authors declare that they have no known competing financial interests or personal relationships that could have appeared to influence the work reported in this paper.

Data availability

Data will be made available on request.

Acknowledgements

This work was supported by the National Research Foundation of Korea (NRF) grant funded by the Korean government (MSIT) (No. 2019R1A2C2088719). K.W. and T.T. acknowledge support from the Elemental Strategy Initiative conducted by the MEXT, Japan, Grant Number JPMXP0112101001, JSPS KAKENHI Grant Numbers JP20H00354 and the CREST (JPMJCR15F3), JST.

Appendix B. Supplementary data

Supplementary data to this article can be found online at https://doi.org/10.1016/j.mssp.2022.107133.

References

[1] G. Fiori, F. Bonaccorso, G. Iannaccone, T. Palacios, D. Neumaier, A. Seabaugh, S. K. Banerjee, L. Colombo, Electronics based on two-dimensional materials, Nat. Nanotechnol. 9 (2014) 768–779.

[2] J. Kim, A. Venkatesan, H. Kim, Y. Kim, D. Whang, G.H. Kim, Improved contact resistance by a single atomic layer tunneling effect in $WS_2/MoTe_2$ heterostructures, Adv. Sci. 8 (2021), e2100102.

[3] S. Yuan, X. Luo, H.L. Chan, C. Xiao, Y. Dai, M. Xie, J. Hao, Room-temperature ferroelectricity in $MoTe_2$ down to the atomic monolayer limit, Nat. Commun. 10 (2019) 1775.

[4] X.J. Yan, Y.Y. Lv, L. Li, X. Li, S.H. Yao, Y. Chen, Bin, X.P. Liu, H. Lu, M.H. Lu, Y. F. Chen, Investigation on the phase- transition-induced hysteresis in the thermal transport along the c-Axis of $MoTe_2$, npj Quantum Mater 2 (2017) 31.

[5] Y.-J. Zhang, R.-N. Wang, G.-Y. Dong, S.-F. Wang, G.-S. Fu, J.-L. Wang, Mechanical properties of 1T-,1T'-, and 1H-MX_2 monolayers and their 1H/1T'-MX_2 (M = Mo, W and X = S, Se, Te) heterostructures, AIP Adv. 9 (2019), 125208.

[6] C. Quan, C. Lu, C. He, X. Xu, Y. Huang, Q.Y. Zhao, X.L. Xu, Band Alignment of $MoTe_2/MoS_2$ nanocomposite films for enhanced nonlinear optical performance, Adv. Mater. Interfac. 6 (2019), 1801733.

[7] M. Wang, D. Li, K. Liu, Q. Guo, S. Wang, X. Li, Nonlinear optical imaging, precise layer thinning, and phase engineering in $MoTe_2$ with femtosecond laser, ACS Nano 14 (2020) 11169–11177.

[8] C. Ruppert, O.B. Aslan, T.F. Heinz, Optical properties and band gap of single- and few-layer $MoTe_2$ crystals, Nano Lett. 14 (2014) 6231–6236.

[9] D. Puotinen, R.E. Newnham, The crystal structure of $MoTe_2$, Acta Crystallogr. 14 (1961) 691.

[10] R. Clarke, E. Marseglia, H.P. Hughes, A low-temperature structural phase transition in β-$MoTe_2$, Philos. Mag. B 38 (1978) 121–126.

[11] D.H. Keum, S. Cho, J.H. Kim, D.H. Choe, H.J. Sung, M. Kan, H. Kang, J.Y. Hwang, S.W. Kim, H. Yang, K.J. Chang, Y.H. Lee, Bandgap opening in few-layered monoclinic $MoTe_2$, Nat. Phys. 11 (2015) 482–486.

[12] R. Sankar, G.N. Rao, I.P. Muthuselvam, C. Butler, N. Kumar, G.S. Murugan, C. Shekhar, T.R. Chang, C.Y. Wen, C.W. Chen, W.L. Lee, M.T. Lin, H.T. Jeng, C. Felser, F.C. Chou, Polymorphic layered $MoTe_2$ from semiconductor, topological insulator, to weyl semimetal, Chem. Mater. 29 (2017) 699–707.

[13] X. Luo, F.C. Chen, J.L. Zhang, Q.L. Pei, G.T. Lin, W.J. Lu, Y.Y. Han, C.Y. Xi, W. H. Song, Y.P. Sun, T_d-$MoTe_2$: a possible topological superconductor, Appl. Phys. Lett. 109 (2016), 102601.

[14] L. Zhou, K. Xu, A. Zubair, A.D. Liao, W. Fang, F. Ouyang, Y.H. Lee, K. Ueno, R. Saito, T. Palacios, J. Kong, M.S. Dresselhaus, Large-area synthesis of high-quality uniform few-layer $MoTe_2$, J. Am. Chem. Soc. 137 (2015) 11892–11895.

[15] L. Yin, X.Y. Zhan, K. Xu, F. Wang, Z.X. Wang, Y. Huang, Q.S. Wang, C. Jiang, J. He, Ultrahigh sensitive $MoTe_2$ phototransistors driven by carrier tunneling, Appl. Phys. Lett. 108 (2016), 043503.

[16] Y. Guo, D. Liu, J. Robertson, 3D behavior of Schottky barriers of 2D transition-metal, ACS Appl. Mater. Interfaces 7 (2015) 25709–25715.

[17] M.J. Mleczko, A.C. Yu, C.M. Smyth, V. Chen, Y.C. Shin, S. Chatterjee, Y.C. Tsai, Y. Nishi, R.M. Wallace, E. Pop, Contact engineering high-performance n-type $MoTe_2$ transistors, Nano Lett. 19 (2019) 6352–6362.

[18] D. Qi, Q. Wang, C. Han, J. Jiang, Y. Zheng, W. Chen, W. Zhang, A.T.S. Wee, Reducing the Schottky barrier between few-layer $MoTe_2$ and gold, 2D Mater. 4 (2017), 045016.

[19] C. Kim, I. Moon, D. Lee, M.S. Choi, F. Ahmed, S. Nam, Y. Cho, H.J. Shin, S. Park, W. J. Yoo, Fermi level pinning at electrical metal contacts of monolayer molybdenum dichalcogenides, ACS Nano 11 (2017) 1588–1596.

[20] Z. Yang, C. Kim, K.Y. Lee, M. Lee, S. Appalakondaiah, C.H. Ra, K. Watanabe, T. Taniguchi, K. Cho, E. Hwang, J. Hone, W.J. Yoo, A fermi-level-pinning-free 1D electrical contact at the intrinsic 2D MoS_2–metal junction, Adv. Mater. 31 (2019), e1808231.

[21] S. Das, H.-Y. Chen, A.V. Penumatcha, J. Appenzeller, High performance multilayer MoS_2 transistors with scandium contacts, Nano Lett. 13 (2013) 100–105.

[22] L. Yang, K. Majumdar, H. Liu, Y. Du, H. Wu, M. Hatzistergos, P.Y. Hung, R. Tieckelmann, W. Tsai, C. Hobbs, P.D. Ye, Chloride molecular doping technique on 2D materials: WS_2 and MoS_2, Nano Lett. 14 (2014) 6275–6280.

[23] S.S. Chee, D. Seo, H. Kim, H. Jang, S. Lee, S.P. Moon, K.H. Lee, S.W. Kim, H. Choi, M.H. Ham, Lowering the Schottky barrier height by graphene/Ag electrodes for high-mobility MoS_2 field-effect transistors, Adv. Mater. 31 (2019), e1804422.

[24] Y. Liu, J. Guo, E. Zhu, L. Liao, S.J. Lee, M. Ding, I. Shakir, V. Gambin, Y. Huang, X. Duan, Approaching the Schottky–Mott limit in van der Waals metal–semiconductor junctions, Nature 557 (2018) 696.

[25] S. Cho, S. Kim, J.H. Kim, J. Zhao, J. Seok, D.H. Keum, J. Baik, D.H. Choe, K. J. Chang, K. Suenaga, S.W. Kim, Y.H. Lee, H. Yang, Phase patterning for ohmic homojunction contact in $MoTe_2$, Science 349 (2015) 625–628.

[26] Q. Liu, J.J. Li, D. Wu, X.Q. Deng, Z.H. Zhang, Z.Q. Fan, K.Q. Chen, Gate-controlled reversible rectifying behavior investigated in a two-dimensional MoS_2 diode, Phys. Rev. B 104 (2021), 045412.

[27] Z.Q. Fan, X.W. Jiang, J.W. Luo, L.Y. Jiao, R. Huang, S.S. Li, L.W. Wang, In-plane Schottky-barrier field-effect transistors based on 1T/2H heterojunctions of transition-metal dichalcogenides, Phys. Rev. B 96 (2017), 165402.

[28] Z.Q. Fan, Z.H. Zhang, S.Y. Yang, High-performance 5.1 nm in-plane Janus WSeTe Schottky barrier field effect transistors, Nanoscale 12 (2020) 21750–21756.

[29] R. Ma, H. Zhang, Y. Yoo, Z.P. Degregorio, L. Jin, P. Golani, J. Ghasemi Azadani, T. Low, J.E. Johns, L.A. Bendersky, A.V. Davydov, S.J. Koester, $MoTe_2$ lateral homojunction field-effect transistors fabricated using flux-controlled phase engineering, ACS Nano 13 (2019) 8035–8046.

[30] X. Zhang, Z. Jin, L. Wang, J.A. Hachtel, E. Villarreal, Z. Wang, T. Ha, Y. Nakanishi, C.S. Tiwary, J. Lai, L. Dong, J. Yang, R. Vajtai, E. Ringe, J.C. Idrobo, B.I. Yakobson, J. Lou, V. Gambin, R. Koltun, P.M. Ajayan, Low contact barrier in 2H/1T' $MoTe_2$ in-plane heterostructure synthesized by chemical vapor deposition, ACS Appl. Mater. Interfaces 11 (2019) 12777–12785.

[31] G.Y. Bae, J. Kim, J. Kim, S. Lee, E. Lee, $MoTe_2$ field-effect transistors with low contact resistance through phase tuning by laser irradiation, Nanomaterials 11 (2021) 2805.

[32] J. Kang, D. Sarkar, W. Liu, D. Jena, K. Banerjee, A Computational Study of Metal-Contacts to Beyond-Graphene 2D Semiconductor Materials 2012 International Electron Devices Meeting, 2012, pp. 17.4.1–17.4.4.

[33] L. Wang, I. Meric, P.Y. Huang, Q. Gao, Y. Gao, H. Tran, T. Taniguchi, K. Watanabe, L.M. Campos, D.A. Muller, J. Guo, P. Kim, J. Hone, K.L. Shepard, C.R. Dean, One-dimensional electrical contact to a two-dimensional material, Science 342 (2013) 614–617.

[34] S.G. Xu, Z.F. Wu, H.H. Lu, Y. Han, G. Long, X.L. Chen, T.Y. Han, W.G. Ye, Y.Y. Wu, J.X.Z. Lin, J.Y. Shen, Y. Cai, Y.H. He, F. Zhang, R. Lortz, C. Cheng, N. Wang, Universal low-temperature Ohmic contacts for quantum transport in transition metal dichalcogenides, 2D Mater. 3 (2016), 021007.

[35] H.Y. Le Thi, M.A. Khan, V. Annadurai, K. Watanabe, T. Taniguchi, G.H. Kim, High-performance ambipolar MoS_2 transistor enabled by indium edge contacts, Nanotechnology 32 (2021), 215701.

[36] Y. Wang, J.C. Kim, R.J. Wu, J. Martinez, X. Song, J. Yang, F. Zhao, A. Mkhoyan, H. Y. Jeong, M. Chhowalla, Van der Waals contacts between three-dimensional metals and two-dimensional semiconductors, Nature 568 (2019) 70–74.

[37] D.S. Schulman, A.J. Arnold, S. Das, Contact engineering for 2D materials and devices, Chem. Soc. Rev. 47 (2018) 3037.

[38] K. Sakanashi, H. Ouchi, K. Kamiya, P. Krüger, K. Miyamoto, T. Omatsu, K. Ueno, K. Watanabe, T. Taniguchi, J.P. Bird, N. Aoki, Investigation of laser-induced-metal phase of $MoTe_2$ and its contact property via scanning gate microscopy, Nanotechnology 31 (2020), 205205.

[39] Y. Tan, F. Luo, M. Zhu, X. Xu, Y. Ye, B. Li, G. Wang, W. Luo, X. Zheng, N. Wu, Y. Yu, Controllable 2H-to-1T′ phase transition in few-layer $MoTe_2$, Nanoscale 10 (2018), 19971.

[40] G.Y. Bae, J. Kim, J. Kim, S. Lee, E. Lee, $MoTe_2$ field-effect transistors with low contact resistance through phase tuning by laser irradiation, Nanomaterials 11 (2021) 2805.

[41] N.R. Pradhan, D. Rhodes, S. Feng, Y. Xin, S. Memaran, B.H. Moon, H. Terrones, M. Terrones, L. Balicas, Field-effect transistors based on few-layered α-$MoTe_2$, ACS Nano 8 (2014) 5911–5920.

[42] S. Fathipour, N. Ma, W.S. Hwang, V. Protasenko, S. Vishwanath, H.G. Xing, H. Xu, D. Jena, J. Appenzeller, A. Seabaugh, Exfoliated multilayer $MoTe_2$ field-effect transistors, Appl. Phys. Lett. 105 (2014), 192101.

[43] M. Grzeszczyk, K. Gołasa, M. Zinkiewicz, K. Nogajewski, M.R. Molas, M. Potemski, A. Wysmołek, A. Babiński, Raman scattering of few-layers $MoTe_2$, 2D Mater. 3 (2016), 025010.

[44] S. Aftab, M.W. Iqbal, A.M. Afzal, M.F. Khan, G. Hussain, H.S. Waheed, M. A. Kamran, Formation of an $MoTe_2$ based Schottky junction employing ultra-low and high resistive metal contacts, RSC Adv. 9 (2019), 10017.

[45] A. Anwar, B. Nabet, J. Culp, F. Castro, Effects of electron confinement on thermionic emission current in a modulation doped heterostructure, J. Appl. Phys. 85 (1999) 2663.

[46] J. Wang, Q. Yao, C.W. Huang, X. Zou, L. Liao, S. Chen, Z. Fan, K. Zhang, W. Wu, X. Xiao, C. Jiang, W.W. Wu, High mobility MoS_2 transistor with low Schottky barrier contact by using atomic thick h-BN as a tunneling layer, Adv. Mater. 28 (2016) 8302–8308.

[47] M.A. Khan, S. Rathi, D. Lim, S.J. Yun, D.H. Young, K. Watanabe, T. Taniguchi, G. H. Kim, Gate tunable self-biased diode based on few layered MoS_2 and WSe_2, Chem. Mater. 30 (2018) 1011–1016.

[48] I. Lee, S. Rathi, D. Lim, L. Li, J. Park, Y. Lee, K.S. Yi, K.P. Dhakal, J. Kim, C. Lee, G. H. Lee, Y.D. Kim, J. Hone, S.J. Yun, D.H. Youn, G.H. Kim, Gate-tunable hole and electron carrier transport in atomically thin dual-channel WSe_2/MoS_2 heterostructure for ambipolar field-effect transistors, Adv. Mater. 28 (2016) 9519–9525.

[49] M.H. Doan, Y. Jin, S. Adhikari, S. Lee, J. Zhao, S.C. Lim, Y.H. Lee, Charge transport in MoS_2/WSe_2 van der Waals heterostructure with tunable inversion layer, ACS Nano 11 (2017) 3832–3840.

[50] X. Zhou, X. Hu, S. Zhou, H. Song, Q. Zhang, L. Pi, L. Li, H. Li, J. Lu, T. Zhai, Tunneling diode based on WSe_2/SnS_2 heterostructure incorporating high detectivity and responsivity, Adv. Mater. 30 (2018), 1703286.

[51] D. Qu, X. Liu, F. Ahmed, D. Lee, W.J. Yoo, Self-screened high performance multi-layer MoS_2 transistor formed by using a bottom graphene electrode, Nanoscale 7 (2015), 19273.

[52] F. Ahmed, M.S. Choi, X. Liu, W.J. Yoo, Carrier transport at the metal–MoS_2 interface, Nanoscale 7 (2015) 9222.

[53] J. Jang, Y. Kim, S.S. Chee, H. Kim, D. Whang, G.H. Kim, S.J. Yun, Clean interface contact using a ZnO interlayer for low-contact-resistance MoS2 transistors, ACS Appl. Mater. Interfaces 12 (2020) 5031–5039.